Hydrophobic Matching Mechanism Investigated by Molecular Dynamics Simulations

Horia I. Petrache,*,† Daniel M. Zuckerman,† Jonathan N. Sachs,‡ J. Antoinette Killian,§ Roger E. Koeppe II,|| and Thomas B. Woolf*,†,‡

Departments of Physiology and Biomedical Engineering, The Johns Hopkins University School of Medicine, Baltimore, Maryland 21205, Department of Biochemistry and Membranes, Utrecht University, Utrecht, The Netherlands, and Department of Chemistry, University of Arkansas, Fayetteville, Arkansas 72701

Received August 21, 2001. In Final Form: November 7, 2001

Membrane protein structure and function are influenced by the interaction with the lipid bilayer environment. The lipid bilayer structure and dynamics are in turn perturbed by the protein insertion. To study this mechanism, a number of experimental studies have used a series of model peptides (WALP) which consist of sequences of alternating alanine and leucine amino acids terminated by a pair of tryptophans at both ends. It has been shown that, due to hydrophobic mismatch, these peptides can assume tilted conformations with respect to the bilayer normal and also perturb the bilayer thickness. In an attempt to rationalize experimental results we performed a series of all-atom molecular dynamics simulations comprising five WALP lengths (16, 17, 19, 21, and 23 residues) and two lipid types (dimyristoyl- and dipalmitoylphosphatidylcholine). The peptide:lipid ratio was in all cases 1:30. We find that the bilayer boundary thickness increases monotonically with WALP length, as expected based on the WALP hydrophobicity. Other structural properties, including peptide tilt, appear to also be modulated by the tryptophan arrangement around the helical axis. These results suggest an important role for tryptophan−environment interactions in both microscopic and mesoscopic properties of the lipid bilayer. We discuss the role of the lipid bilayer density gradient on the dynamic structure of the peptide−lipid bilayer system and show the dependence of peptide side chain interactions and side chain volumes on the location along the bilayer normal. We find that WALP sequences with the tryptophan residues on opposite sides of the helix have an overall looser packing with the surrounding lipids and larger peptide tilts than peptides with the tryptophans on the same side.

Introduction

Membrane proteins function within a complex heterogeneous environment that differs markedly from the aqueous medium of globular proteins. Significant progress has been made toward understanding some of the key characteristics of both lipids and membrane proteins which determine the favorable energetics of this environment.[1−3] A classical description of transmembrane protein−lipid bilayer interactions is the "mattress model" proposed by Mouritsen and Bloom.[4] In this description, the hydrophobic span of the lipid bilayer and the protein are modeled as springs with different force constants and equilibrium lengths, and the coupling between the springs is expressed as a function of length mismatch. The equilibrium structure is achieved at spring deformations for which the total free energy is minimal. In this framework, the energetics of the protein−lipid bilayer system are described as *mechanical* deformations of both protein and lipid molecules, the relative magnitude of the deformations depending on the material properties of the molecular constituents. The mattress model treats the bilayer thickness and the peptide length as the dominant degrees of freedom that dictate the structural matching within the membrane. Bilayer−protein models have since evolved to include additional degrees of freedom, such as bilayer curvature[5−9] and recently lipid tilt.[10] The common feature of these models is the continuum, elastic description of the lipid bilayer, which is represented as an elastic plate (slab), characterized by compressibility and bending moduli.[11,12] Finding the most probable membrane state (shape) then amounts to the minimization of the deformation free energy functional subject to boundary conditions at the peptide−lipid interface. It is important to note that because it involves structural deformations, the structural matching mechanism may be implicated in conformational changes associated with protein function.[13,14] As for all elastic materials, structural deformations can be viewed as a source of potential energy that may be utilized by the membrane system to assist with a biological process.[15−17]

* Corresponding authors: H.I.P., current address LPSB/NICHD, National Institutes of Health, Bldg 12A, Rm 2041, Bethesda, MD 20892, tel. 301-402-4698, fax 301-402-9462, E-mail horia@helix.nih.gov; T.B.W., Department of Physiology, Johns Hopkins University School of Medicine, Baltimore, MD 21205, tel. 410-614-2643, fax 410-614-4436, E-mail woolf@groucho.med.jhmi.edu.

† Department of Physiology, The Johns Hopkins University School of Medicine.

‡ Department of Biomedical Engineering, The Johns Hopkins University School of Medicine.

§ Utrecht University.

|| University of Arkansas.

(1) Bloom, M.; Evans, E.; Mouritsen, O. G. *Q. Rev. Biophys.* **1991**, *24*, 293−397.
(2) White, S. H.; Wimley, W. C. *Annu. Rev. Biophys. Biomol. Struct.* **1999**, *28*, 319−365.
(3) Killian, J. A.; Heijne, G. V. *Trends Biochem. Sci.* **2000**, *25*, 429−434.
(4) Mouritsen, O. G.; Bloom, M. *Biophys. J.* **1984**, *46*, 141−153.
(5) Huang, H. W. *Biophys. J.* **1986**, *50*, 1061−1070.
(6) Helfrich, P.; Jakobsson, E. *Biophys. J.* **1990**, *57*, 1075−1084.
(7) Dan, N.; Safran, S. A. *Biophys. J.* **1998**, *75*, 1410−1414.
(8) Nielsen, C.; Goulian, M.; Andersen, O. S. *Biophys. J.* **1998**, *74*, 1966−1983.
(9) Nielsen, C.; Andersen, O. S. *Biophys. J.* **2000**, *79*, 2583−2604.
(10) May, S. *Eur. Biophys. J.* **1999**, *29*, 17−28.
(11) de Gennes, P. G. *The Physics of Liquid Crystals*; Clarendon Press: Oxford, U.K., 1974.
(12) Leibler, S. *J. Phys.* **1986**, *47*, 507−516.
(13) Lundbæk, J. A.; Birn, P.; Girshman, J.; Hansen, A. J.; Andersen, O. S. *Biochemistry* **1996**, *35*, 3825−3830.
(14) Dumas, F.; Lebrun, M. C.; Tocanne, J.-F. *FEBS Lett.* **1999**, *458*, 271−277.

10.1021/la011338p CCC: $22.00
Published on Web 01/26/2002

The body of current experimental data, while supporting elastic models, still lacks direct information on the peptide−lipid interface. The quantities measured by both structural[18,19] and energetic techniques[20−23] are averages over the whole system. As such, additional assumptions and modeling are needed to interpret these averages in terms of local deformations. On this level, many fundamental questions regarding hydrophobic matching still require attention: (i) What is the precise molecular packing at the peptide−lipid interface? (ii) What distinguishes boundary lipids from bulk lipids? (iii) What is the deformation of the protein itself? Molecular dynamics simulations in which molecules are represented in atomic detail have the potential to address these issues.[24−30] Despite limited sampling, computer simulations have significantly contributed to our understanding of molecular processes, even on biologically relevant scales, by enabling the qualitative and often quantitative interpretation of experimental results. The value of molecular dynamics resides not only in the detailed description of the average membrane structure but also in the calculated fluctuation data, the latter being related to thermodynamic quantities such as entropy, heat capacities, and thermal compressibilities.[31−33]

One family of peptides that has been extensively used in experimental studies of the hydrophobic matching mechanism are constructed as sequences of alternating Leu and Ala residues of various lengths, terminated by one pair of Trp residues at each end.[18,34,35] These peptides are denoted as WALP*n*, where *n* represents the number of amino acids. For instance, WALP17 is formyl-Ala-Trp-Trp-(Leu-Ala)$_5$-Leu-Trp-Trp-Ala-ethanolamine. The central Ala-Leu repeats are strongly hydrophobic and force the peptides to partition into the lipid bilayer, where they form stable α-helices.[18,35] The Trp pairs are added to the peptide ends due to the abundance of these residues in the interfacial regions of membrane proteins.[36] It has been suggested that the bulky Trp residues act to stabilize the transmembrane orientation of the peptide, by having a strong preference for the lipid−water interfacial region.[37−40] The presence of tryptophan residues in the WALP sequence is therefore expected to have a major impact on structural deformations caused by hydrophobic peptide−lipid matching.

The goal of this work is to investigate the hydrophobic matching mechanism by an extensive series of explicit (all-atom) molecular dynamics simulations of WALP−lipid systems. One recognizes that, in principle, the structural adaptations in peptide−lipid systems depend on many physicochemical factors including peptide and lipid type as well as peptide:lipid concentration, temperature, and hydration level. As a rule, to establish the relative role of all these various factors requires a systematic approach, as shown by de Planque et al.,[18,35,41] who investigated a WALP series incorporated into various lipid bilayers. Working under a similar paradigm, we performed molecular dynamics simulations of five different WALP lengths (16, 17, 19, 21, and 23), each solvated by two different lipid types: dimyristoylphosphatidylcholine (DMPC, 14 carbons/acyl chain); dipalmitoylphosphatidylcholine (DPPC, 16 carbons/acyl chain). The peptide:lipid concentration is in all cases 1:30, as in the experimental work of de Planque et al.[18,35,41] Given the inherent limitations of molecular dynamics simulations (as will be discussed in more detail later), we chose to simulate and compare a series of similar systems, as we have previously done for investigating helix−helix interactions within lipid bilayers.[30] As such, a contrast of the whole WALP series within simulations as well as between simulation and experiment is more meaningful than a point-by-point comparison between individual systems.

In what follows we show the complexity of structural deformations that occur even in the case of the relatively simple WALP sequences. We first present results for the peptide tilt angle together with the bilayer thickness deformations. We then show more detailed bilayer structural properties, with regard to boundary conditions at the peptide−lipid interface, including the bilayer slope and asymmetry. The discussion of these results leads to consideration of Trp arrangements around the helix axis, and we show that the bulky Trp side chains have a relatively long-range effect on the bilayer structure rather than simply creating a local perturbation. By taking the perspective of the density gradient along the bilayer normal, we conclude that structural adaptations of the protein insertion and the hosting lipid are strongly influenced by the nature and position of peptide residues within the bilayer.

Methods

Simulations of small bilayer patches were performed using CHARMM version 26.[42] Each system consists of one peptide plus 15 lipids/monolayer (30 lipids in total) and a corresponding

(15) Brown, M. F. *Chem. Phys. Lipids* **1994**, *74*, 159−180.
(16) Keller, S. L.; Gruner, S. M.; Gawrisch, K. *Biophys. Biochim. Acta* **1996**, *1278*, 241−246.
(17) Bezrukov, S. M.; Rand, P. R.; Vodyanoy, I.; Parsegian, V. A. *Faraday Discuss.* **1998**, *111*, 173−183.
(18) de Planque, M. R. R.; Greathouse, D. V.; Koeppe, R. E.; Schäfer, H.; Marsh, D.; Killian, J. A. *Biochemistry* **1998**, *37*, 9333−9345.
(19) Harroun, T. A.; Heller, W. T.; Weiss, T. M.; Yang, L.; Huang, H. W. *Biophys. J.* **1999**, *76*, 937−945.
(20) Jost, P. C.; Griffith, O. H.; Capaldi, R. A.; Vanderkooi, G. *Proc. Natl. Acad. Sci. U.S.A.* **1973**, *70*, 480−484.
(21) Boggs, J. M.; Moscarello, M. A. *Biochemistry* **1978**, *17*, 5734−5739.
(22) Rehorek, M.; Dencher, N. A.; Heyn, M. P. *Biochemistry* **1985**, *24*, 5980−5988.
(23) Davies, S. M. A.; Epand, R. F.; Bradshaw, J. P.; Epand, R. M. *Biochemistry* **1998**, *37*, 5720−5729.
(24) Woolf, T. B.; Roux, B. *Proc. Natl. Acad. Sci.U.S.A.* **1994**, *91*, 11631−11635.
(25) Woolf, T. B.; Roux, B. *Proteins: Struct., Funct., Genet.* **1996**, *24*, 92−114.
(26) Woolf, T. B. *Biophys. J.* **1997**, *73*, 2376−2392.
(27) Woolf, T. B. *Biophys. J.* **1998**, *74*, 115−131.
(28) Tieleman, D. P.; Forrest, L. R.; Sansom, M. S. P. *Biochemistry* **1998**, *37*, 17554−17561.
(29) Chiu, S.-W.; Subramaniam, S.; Jakobsson, E. *Biophys. J.* **1999**, *76*, 1929−1938.
(30) Petrache, H. I.; Grossfield, A.; MacKenzie, K. R.; Engelman, D. M.; Woolf, T. B. *J. Mol. Biol.* **2000**, *302*, 727−746.
(31) Edholm, O.; Berendsen, H. J. C.; van der Ploeg, P. *Mol. Phys.* **1983**, *48*, 379−388.
(32) Heimburg, T. *Biochim. Biophys. Acta* **1998**, *1415*, 147−162.
(33) Feller, S. E.; Pastor, R. W. *J. Chem. Phys.* **1999**, *111*, 1281−1287.
(34) Killian, J. A.; Salemink, I.; de Planque, M. R. R.; Lindblom, G.; Koeppe, R. E.; Greathouse, D. V. *Biochemistry* **1996**, *35*, 1037−1045.
(35) de Planque, M. R. R.; Goormaghtigh, E.; Greathouse, D. V.; Koeppe, R. E.; Kruijtzer, J. A. W.; Liskamp, R. M. J.; de Kruijff, B.; Killian, J. A. *Biochemistry* **2001**, *40*, 5000−5010.
(36) Wallin, E.; Tsukihara, T.; Yoshikawa, S.; von Heijne, G.; Elofsson, A. *Protein Sci.* **1997**, *6*, 808−815.
(37) Yau, W.-M.; Wimley, W. C.; Gawrisch, K.; White, S. H. *Biochemistry* **1998**, *37*, 14713−14718.
(38) Persson, S.; Killian, J. A.; Lindblom, G. *Biophys. J.* **1998**, *75*, 1365−1371.
(39) Braun, P.; von Heijne, G. *Biochemistry* **1999**, *38*, 9778−9782.
(40) Mall, S.; Broadbridge, R.; Sharma, R. P.; Lee, A. G.; East, J. M. *Biochemistry* **2000**, *39*, 2071−2078.
(41) de Planque, M. R. R.; Kruijtzer, J. A. W.; Liskamp, R. M. J.; Marsh, D.; Greathouse, D. V.; Koeppe, R. E.; de Kruijff, B.; Killian, J. A. *J. Biol. Chem.* **1999**, *30*, 20839−20846.
(42) Brooks, B. R.; Bruccoleri, R. E.; Olafson, B. D.; States, D. J.; Swaminathan, S.; Karplus, M. *J. Comput. Chem.* **1983**, *4*, 187−217.

Table 1. Simulation Setup

lipid[a]	*T*/°C	area/lipid[b]	waters/lipid	tot. area[b]	tot. waters
DMPC[c]	30	59.7	25.7	1112	957
DPPC[d]	50	62.9	29.1	1160	1070

[a] Each simulation contains 30 lipids and 1 WALP sequence. [b] The units for the area are Å^2. [c] Reference 50. [d] Reference 51.

number of waters, as given in Table 1. Periodic boundary conditions were used with constant number of atoms (N), temperature (T), lateral area (A), and normal pressure (P_N) to generate NAP_NT ensembles. Due to the presence of a surface tension at the lipid water interface, the choice of the simulated ensemble for lipid bilayers is a delicate issue, as discussed by Jähnig.[43] In particular, it has been argued that a significant surface tension (on the order of 10−50 dyn/cm) develops in a lipid bilayer patch that consists of a small number of lipid molecules.[44,45] The natural simulation ensemble will then be $N\gamma P_NT$, where γ stands for constant surface tension. The complication, however, arises from the lack of a priori knowledge of the value of γ, which in principle depends on the bilayer type and system size. For the WALP−lipid systems, we have found that a misassignment of the surface tension readily leads to unstable membrane structures. As we aim for a straightforward comparison across the WALP series, we choose constant area simulations, thereby providing a consistent baseline for the comparison. As further justification, having generated constant-area ensembles, the surface tensions can be calculated and used for subsequent constant surface tension simulations. Another noticeable advantage of constant area simulations is faster equilibration, which facilitates our approach of multiple simulations. We have therefore employed the relatively more rigid NAP_NT ensemble for a starting point in a systematic, comparative analysis of the WALP series. The area of each simulation box (A_{box}) has been chosen as explained below. Note that even if the lateral area is fixed during the simulation, the volume of the simulation cell in a NAP_NT run is not; the vertical dimension of the cell is free to fluctuate under the constant normal pressure constraint, and consequently, the densities of the different molecular components are free to adjust. In addition, the lateral area can redistribute among the peptide and the lipid molecules, even under the constraint $A_{box} = A_P + N_L A_L =$ constant, where N_L represents the number of lipids in one monolayer. We can therefore compare the dynamics of the area/peptide, A_P, and of the area/lipid, A_L, across the various simulations.

Two different lipid types were considered: DMPC (dimyristoylphosphatidylcholine); DPPC (dipalmitoylphosphatidylcholine). Simulation temperatures were 30 °C for DMPC and 50 °C for DPPC systems, as at these temperatures the lipids are in the fluid state. The normal pressure P_N was set to 1 atm for all systems, while the lateral area was set to different values for the two lipids, as given in Table 1. The number of water molecules in each case was determined starting from experimental measurements on fully hydrated multilamellar vesicles of pure lipid bilayers. Specifically, using the number of waters/lipid and the lipid cross-sectional area in each lipid bilayer, the number of waters/unit area was calculated and then scaled to the total area of the simulation box (see ref 30 for an extended discussion on hydration level). The total area of the simulation box should include the lateral area occupied by the peptide molecule. It is important to realize that peptide area is not an intrinsic property of the peptide but depends on the specific packing within the lipid bilayer. However, we have estimated the peptide area as follows. First, the peptide volumes were estimated by calculating the excluded volume for a spherical probe the size of a water molecule. These volumes were then divided by effective helix lengths to obtain "bare" cross-sectional areas. Tilt averaged areas were estimated by considering a uniform population of peptide tilt angles between 0 and 25°.[46] These results were combined with the "collapsed" area obtained by translating all atoms along the helix axis in the $z = 0$ plane. Finally, an average value of ∼216 Å^2 was calculated and used for all WALP simulations, both in DMPC and DPPC. To these results we added the area/lipid measured experimentally at full hydration, to obtain the total area of each simulation box. This choice was based on the principle of minimizing the total number of free parameters, so that the simulation box area (A_{box}) was the same for a given lipid.

Initial membrane structures were constructed using the methodology developed by Woolf and Roux,[24,25] as explained below. The starting WALP structures were generated by molecular modeling as described previously,[47] while lipid molecules were randomly chosen from a library of preequilibrated lipids in the fluid state. The DPPC library was provided by R. W. Pastor[48] and also used to generate DMPC molecules by deletion of two terminal carbon segments from each acyl chain. The lipid placement around the peptide was first determined by a 100 ps simulation of large van der Waals (vdW) spheres constrained in the vicinity of two parallel planes at the average location of the lipid headgroups. Next, lipid molecules were randomly chosen from the libraries and placed at the location of the vdW spheres. The lipids were then systematically rotated and translated around the initial positions, to reduce the number of steric collisions, followed by a gradual increase of the vdW atom radii and minimization. During this minimization stage, the peptide atoms were kept fixed to their initial locations (zero backbone tilt), and the lipid glycerol C2 atoms were restrained to their initial plane using a harmonic potential of 10 kcal mol^{-1} Å^{-2} and a cutoff of 1 Å. At least 12 configurations were generated for each system by reselecting from the lipid library and repeating the equilibration steps. The resulting configurations were screened for characteristic properties of lipid bilayers in the fluid state (such as acyl chain and headgroup order), and the best structure was selected in each case. Such a rational approach to building a bilayer in the fluid state significantly minimizes the equilibration time. Next, a TIP3 water overlay was performed from the glycerol regions on both sides of the membrane, and periodic boundary conditions were set in all three spatial directions. Water−lipid packing was first relaxed by a series of minimization and Langevin dynamics simulations with a friction coefficient of 5 ps^{-1}, followed by velocity scaling simulations with electrostatics shifted and van der Waals switched at 12 Å. Next, the constraints on the lipid glycerols were removed, and equilibration continued with 25 ps of leapfrog constant pressure and constant-temperature dynamics. In the next stage of equilibration, the peptide restraints were removed and 25 ps of dynamics was performed using the particle mesh Ewald method for electrostatic interactions.[49] A cutoff of 12 Å was used for van der Waals interactions.[33] The time step was 2 fs, and all bonds involving hydrogens were fixed using the SHAKE algorithm, with a tolerance (relative deviation) of 10^{-6}. The frequency of regenerating the nonbonded list was set with a heuristic testing algorithm that updates on the basis of the distance each atom moved since the last list update. Production dynamics simulations for each system were performed for 1.5 ns. The results reported in this paper use the conformations generated after a 250 ps equilibration window for each trajectory.

Results

Initial Aspects of WALP−Lipid Systems. Biological systems, and in particular lipid bilayers, are soft materials. In consequence, the expectation is that peptide−membrane interactions lead to structural deformations of both lipid and protein. As mentioned in the Introduction, two major structural parameters are commonly believed to dominate the matching mechanism: *unperturbed* bilayer thickness; *unperturbed* peptide length. Within the current theoretical framework, the case of perfect matching occurs when the two lengths are equal, i.e. the incorporation of

(43) Jähnig, F. *Biophys. J.* **1996**, *71*, 1348−1349.
(44) Feller, S. E.; Pastor, R. W. *Biophys. J.* **1996**, *71*, 1350−1355.
(45) Chiu, S.-W.; Clark, M.; Balaji, V.; Subramaniam, S.; Scott, H. L.; Jakobsson, E. *Biophys. J.* **1995**, *69*, 1230−1245.
(46) Bowie, J. U. *J. Mol. Biol.* **1997**, *5*, 780−789.
(47) van der Wel, P. C. A.; Pott, T.; Morein, S.; Greathouse, D. V.; Koeppe, R. E.; Killian, J. A. *Biochemistry* **2001**, *39*, 3124−3133.
(48) Hardy, B. J.; Pastor, R. W. *J. Comput. Chem.* **1994**, *15*, 208−226.
(49) Sagui, C.; Darden, T. A. *Annu. Rev. Biophys. Biomol. Struct.* **1999**, *28*, 155−179.

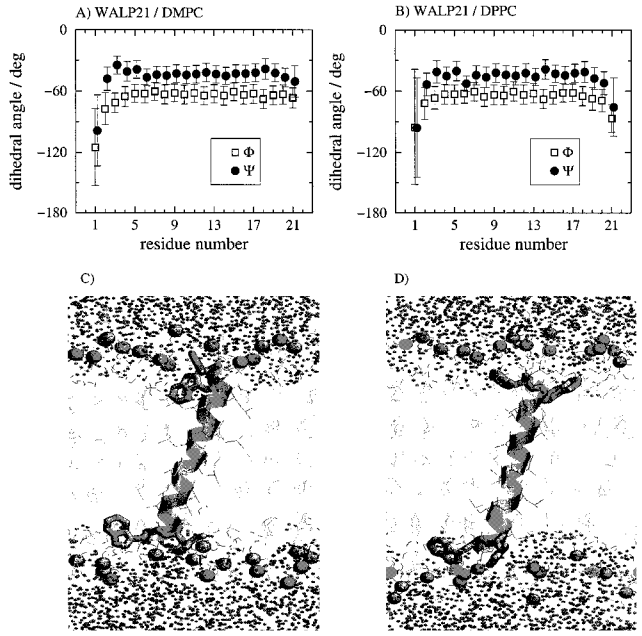

Figure 1. Average peptide backbone dihedral angles Φ (open squares) and Ψ (solid circles) for WALP21 in DMPC (A) and DPPC (B) and root mean-square deviations during the trajectory (shown as fluctuation bars). Panels C and D show snapshots corresponding to (A) and (B), respectively. Highlighted are the Trp residues and the lipid phosphorus atoms. Backbone helical structure is not significantly affected by peptide tilt.

the peptide requires minimal deformation of both peptide and lipid bilayer. With a difference of roughly 2−3 Å between the fluid state bilayer thicknesses of DMPC[50] and DPPC,[51] the WALP lengths that best match the two lipids would be predicted to differ by about 2 residues, if differences in lateral packing (cross-sectional area) are to be ignored. In addition, for each given lipid bilayer, one expects the peptide tilt to increase with increasing peptide length. While some of these expectations are indeed validated by our all-atom molecular dynamics simulations, we will show that structural adaptations of peptide and lipid molecules are rather complex.

Before presentation of the results on peptide tilt and bilayer deformation, let us discuss the peptide helical structure. The backbone structure for one of the simulated peptides (WALP21) is shown in Figure 1 in terms of the dihedral angle averages and mean-square fluctuations during the simulation. All the other peptides have similar behavior (data not shown). The averages and fluctuations are typical for all-atom simulations of helical peptides as obtained by Woolf[26] and Petrache et al.[30] for similar systems and simulation setup. In particular, the amplitude of backbone fluctuations, shown by the mean-square deviation bars in Figure 1, indicate that a significant amount of motion occurs in the nanosecond time scale. The mean-square fluctuations of backbone dihedrals are of about 8−9° with larger values for the end residues. Because of these dihedral fluctuations, the backbone length also fluctuates. Simulation results for the helix lengths between the first and the last Trp residues are given in Table 2 in terms of trajectory averages, L_{WW}, and root mean-square fluctuations, σ_{WW}, and show that thermal fluctuations of helix length are between 1 and 2%. Table 2 also shows that the length/residue is in all

Table 2. Average Helix Length, L_{WW}, and Root-Mean-Square Fluctuations σ_{WW}

lipid	WALP	L_{WW}[a]	σ_{WW}	%[b]	L_{WW}/m[c]	$\sigma_{WW}/\sqrt{m}$	K_L[d]
DMPC	16	19.3	0.30	1.5	1.49	0.08	6.8
(30 °C)	17	20.6	0.33	1.6	1.47	0.09	5.6
	19	23.7	0.28	1.2	1.48	0.07	7.6
	21	27.0	0.45	1.7	1.50	0.11	3.0
	23	29.7	0.34	1.1	1.48	0.08	5.3
DPPC	16	19.5	0.32	1.6	1.50	0.09	6.2
(50 °C)	17	20.8	0.33	1.6	1.49	0.09	5.9
	19	23.8	0.32	1.3	1.49	0.08	6.4
	21	26.8	0.40	1.5	1.49	0.09	4.0
	23	29.5	0.37	1.2	1.48	0.08	4.8

[a] Represents the distance between the C_α carbons of first and last Trp residues, projected on the helix axis. [b] Percent ratio of σ_{WW} to L_{WW}. [c] m represents the number of residues between the first and the last Trp (e.g. $m = 14$ for WALP17). [d] Effective backbone elastic modulus (spring constant) calculated as $K_L = \kappa_B T/\sigma_{WW}^2$ in units of kcal mol^{-1} Å^{-2}. All lengths are in Å units.

cases close to 1.5 Å, the expected value for α-helical structures. Also of note in Table 2 is that the temperature variation of L_{WW} is minimal—compare the results for DMPC and DPPC systems, which are simulated at 30 and 50 °C. Estimated errors are on the order of ±0.01 Å/residue. Using the thermal fluctuation σ_{WW} from Table 2, we can calculate effective "spring constants" for the simulated peptides. The results are on the order of 3−8 kcal mol^{-1} Å^{-2} (see Table 2), indicating relatively rigid backbone structures. Indeed, the peptide backbone is typically more rigid than the lipid bilayer as discussed by Harroun et al.[19] The fact that the backbone length/residue is roughly the same for all peptides in Table 2 (within simulation uncertainty) implies that structural matching between the lipid bilayer and the inserted peptide occurs primarily through variation of other structural parameters, such as peptide tilt and bilayer thickness.

Also shown in Figure 1 are structural snapshots from simulations indicating that the peptide can tilt relative to the bilayer normal while maintaining helical structure. In addition, the snapshots in Figure 1 emphasize the size of the Trp side chains and their location at the lipid−water interface. For peptides situated symmetrically about the mid-bilayer plane, the lengths L_{WW} reported in Table 2 correspond to a distance between 10 and 15 Å toward the lipid−water interface in each monolayer. For *unperturbed* DPPC, this location corresponds to the inner half of the carbonyl distributions.[51] In consequence, if the peptide is centered in the bilayer and the bilayer thickness is not perturbed, the Trp residues would be buried inside the hydrocarbon core and have minimal exposure to water. However, the bilayer *is* perturbed next to the peptide, as we will show below. In addition, because the water−lipid interface is very broad and highly heterogeneous,[52] the Trp interaction with the environment is expected to depend on the exact location along the bilayer normal.[53]

Figure 2 shows the peptide location within the lipid bilayer for the case of WALP21. The time series shown represent the location of three consecutive C_α carbons along the peptide backbone, starting with the outermost Trp residue at each end. The time series are plotted in reference to the average position of lipid phosphorus atoms in each monolayer in each time frame, where the $z = 0$ level (bilayer center) is set by the center of mass of the lipid molecules. The figure emphasizes the stability of the membrane system, after an equilibration period of 250

(50) Petrache, H. I.; Tristram-Nagle, S.; Nagle, J. F. *Chem. Phys. Lipids* **1998**, *95*, 83−94.
(51) Nagle, J. F.; Zhang, R.; Tristram-Nagle, S.; Sun, W.-J.; Petrache, H. I.; Suter, R. M. *Biophys. J.* **1996**, *70*, 1419−1431.
(52) Wiener, M. C.; White, S. H. *Biophys. J.* **1992**, *61*, 434−447.
(53) Grossfield, A.; Woolf, T. B. *Langmuir* **2002**, *18*, 198−210.

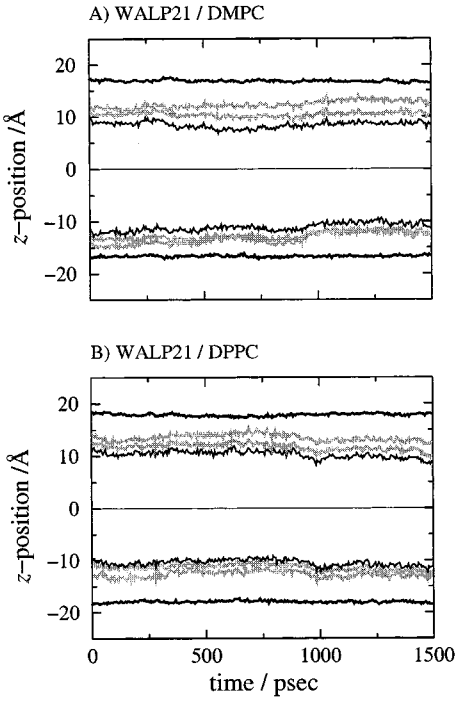

Figure 2. Time series of atom positions along the bilayer normal, corresponding to (bottom to top) lipid P, W2, W3, L4, L18, W19, W20, and lipid P. Lipid phosphorus (P) position represents the average in each monolayer. Peptide residues are represented by the C_α carbons. The times series shown include 250 ps of equilibration not used in the simulation analysis.

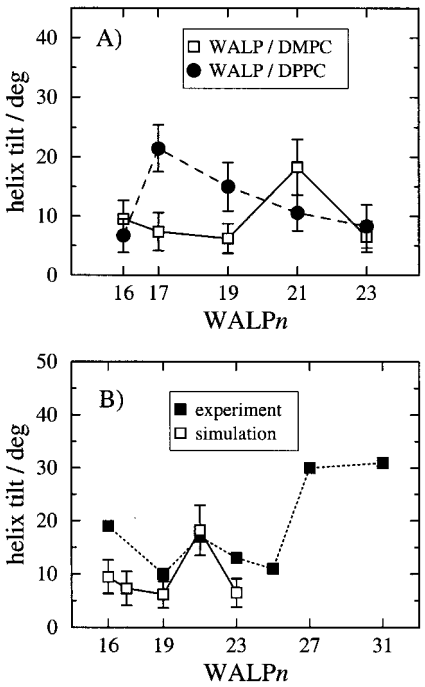

Figure 3. Peptide tilt is not directly correlated with WALP sequence length (*n*). Part A shows trajectory averaged peptide tilt and root-mean-square fluctuations from simulations. Part B compares simulations (open squares) with experimental data (solid squares) on WALP/DMPC systems. Experimental values give maximum tilt angles (upper limits) with an estimated error of ±5° (from ref 35).

ps, when the average bilayer thickness (D_{PP}) becomes practically constant. Individual lipid molecules still undergo significant vertical motion and generate a phosphorus distribution with a width of 3−5 Å, which is typical for lipid bilayers in the fluid phase[54] (data not shown). The time series of backbone C_α locations indicate a rigid-body motion of the peptide along the bilayer normal, with an amplitude of 2−3 Å within the simulation time scale. Faster local fluctuations are observed about this slow rigid-body motion. We should mention that, in addition to the dynamics along the *z* axis, there is a significant degree of peptide motion in the membrane plane that is not evident from Figure 2.

Peptide Tilt Does Not Vary Monotonically with Peptide Length. Peptide tilt relative to the bilayer normal is an important degree of freedom for the relaxation of peptide−lipid bilayer mismatch.[35,55−58] The averages and mean-square fluctuations of helix tilt from our nanosecond simulations are shown in Figure 3A. It is immediately clear that WALP tilt does not vary monotonically with peptide length or degree of mismatch. This is contrary to expectations on the basis of a simple slab model assuming a structureless peptide and lipid bilayer. The largest tilt angles, on the order of 20°, are found for WALP17 in DPPC and WALP21 in DMPC, while the other simulations give smaller angles of about 10°. Figure 3B compares the simulation results with recent experimental measurements of WALP tilt in DMPC bilayers.[35] The experimental results involve a set of assumptions for the interpretation of FTIR data[35,59] but clearly indicate that the tilt depends on more parameters than just the peptide length. Considering the whole span of experimental data (WALP17−31), there is a global increase of the tilt as the peptide sequence increases, but the variation is quite complex, with two apparent local minima.

We emphasize that the present simulation results on the helix tilt should be interpreted qualitatively rather than quantitatively. While the amount of tilt fluctuation is significant during nanosecond time scales (as shown by the mean-square fluctuation bars in Figure 3A), much longer trajectories are needed to fully sample this degree of freedom. In other words, the probability distribution for the tilt angle is in principle a broad distribution. Indeed, in the case of WALP19 and WALP23 in DMPC, for which we have partially analyzed longer trajectories (10 and 5 ns, respectively), we observe large variations of the instantaneous tilt angle. The average tilt however stays within the standard deviation computed from the short (1.25 ns) trajectories. Specifically, for WALP23/DMPC the 5 ns average and standard deviation is 9° ± 4°, compared to 7° ± 3° obtained from the first 1.25 ns, while for WALP19/DMPC we see no significant change going from 1 to 10 ns sampling—at both time scales we obtain 6° ± 3°.

Bilayer Boundary Thickness Increases with Peptide Length. Given the complex tilt behavior, the natural question is how is the bilayer responding to the perturbation imposed by the peptide. Figure 4 shows simulation results for the bilayer thickness. The quantity plotted is the average distance between lipid phosphorus atoms in the two monolayers along the bilayer normal, denoted D_{PP}. From each simulation we have calculated both the overall average, D_{PP}, and the average over boundary lipids

(54) Nagle, J. F.; Tristram-Nagle, S. *Biochim. Biophys. Acta* **2000**, *1469*, 159−195.
(55) Shen, L.; Bassolino, D.; Stouch, T. *Biophys. J.* **1997**, *73*, 3−20.
(56) Killian, J. A. *Biochim. Biophys. Acta* **1998**, *1376*, 401−416.
(57) Forrest, L. R.; Tieleman, D. P.; Sansom, M. S. P. *Biophys. J.* **1999**, *76*, 1886−1896.
(58) Fisher, W. B.; Forrest, L. R.; Smith, G. R.; Sansom, M. S. P. *Biopolymers* **2000**, *53*, 529−538.
(59) Bechinger, B.; Ruysschaert, J.-M.; Goormaghtigh, E. *Biophy. J.* **1999**, *76*, 552−563.

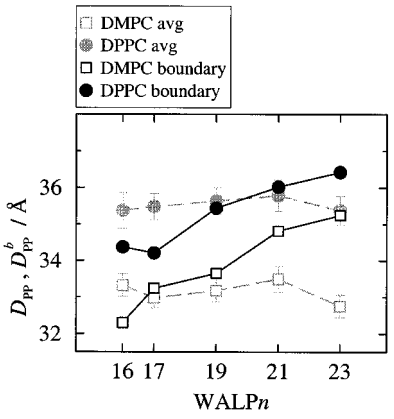

Figure 4. Bilayer thickness adjacent to the peptide (D^b_{PP}) and averaged over the whole simulation box (D_{PP}), as a function of WALP sequence length, *n*. DMPC is shown with open squares, and DPPC is shown with solid circles. The boundary thickness, D^b_{PP} (solid lines), increases monotonically with the peptide length, while the overall average D_{PP} (dashed gray) shows deviations at the shortest and the longest peptide length.

only, denoted by D^b_{PP}. As expected, the boundary thickness, D^b_{PP} increases with WALP sequence length *n*. This corresponds to the case of tight hydrophobic coupling (no slip) between the inclusion (peptide) and the lipid bilayer.[8,19] The overall average D_{PP}, however, shows a weaker dependence with peptide length because it also includes the lipids away from the peptide and, therefore, depends on the exact bilayer shape.[19] For WALP lengths of 17, 19, and 21, D_{PP} increases monotonically, but we do find deviations at the lowest and highest peptide lengths (16 and 23, respectively). While the behavior of D^b_{PP} can be predicted on the basis of the peptide length, the behavior of the overall average bilayer thickness is more complex and depends on the peptide:lipid concentration. The results in Figure 4, obtained at a concentration of 1:30, suggest an interesting picture of the lipid bilayer elasticity. Namely, as the boundary thickness, D^b_{PP}, is modified by the peptide, the thickness away from the lipid−peptide interface changes in the opposite way and keeps the overall change in D_{PP} small. This compensatory mechanism, which may be enhanced by the constant-area constraint, can be regarded as a seesaw behavior sustained by the mesoscopic viscosity of the lipid bilayer.[60] Recall that the present calculations are carried out at high peptide concentration and therefore the distance from one peptide to the next is small, on the order of 30 Å. More dilute systems might allow lipids far away from the peptide to relax to the unperturbed (pure lipid) bilayer thickness, D^∞_{PP}. In general, even for dilute systems, one might expect the bilayer perturbation profile to go through an inflection point before reaching the unperturbed thickness.[7−9,19,61] This is opposed to a smooth, monotonic decay from D^b_{PP} to D^∞_{PP}. As a rule, the exact profile is ultimately determined by the particular elasticity constants and inclusion dimensions in each case, as discussed by Nielsen et al.[8]

Another interesting observation can be made by comparing these results on D^b_{PP} with the results on the helix tilt from the previous figure. As can be seen in Figure 3A, the average tilt angles for WALP16 and WALP23 are comparable in magnitude. In contrast, D^b_{PP} for these two peptides varies by a significant amount: 2.95 Å (DMPC); 2.06 Å (DPPC). Apparently, it is easier to deform the bilayer locally than to tilt the peptide. The variation of D^b_{PP} with peptide length that we obtain is comparable with previous estimates based on experimental measurements.[18,41]

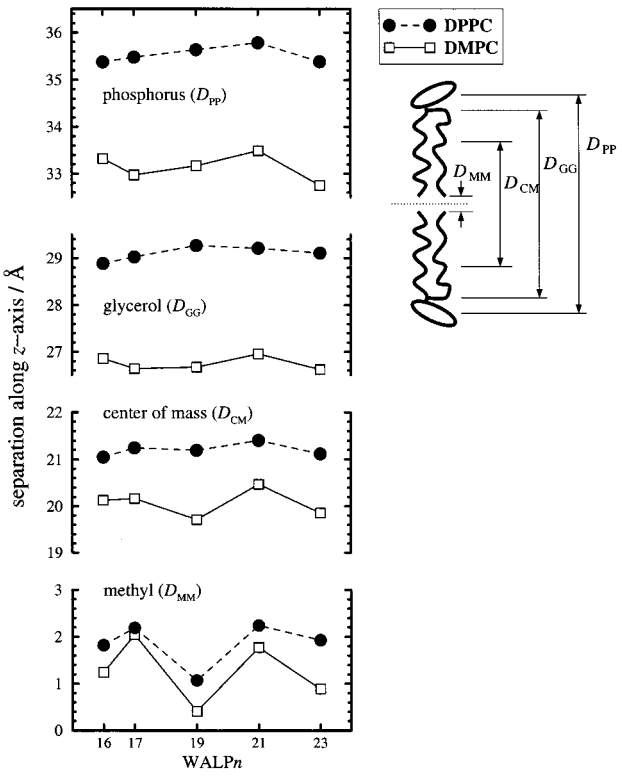

Figure 5. Average separation distances along the bilayer normal for lipid phosphorus atoms (D_{PP}), glycerol C_2 carbons (D_{GG}), lipid centers of mass (D_{CM}), and acyl chain terminal methyls (D_{MM}), as illustrated by the cartoon on the right. There is a nonlocal helical effect as a function of WALP sequence length *n*, extending across the entire bilayer depth.

It is worth keeping in mind that all-atom computer simulations are typically limited in both length and time scale. One should, therefore, be cautious when making quantitative comparison between the results presented above and experiment. Even at this stage, however, there is a qualitative agreement between our simulations and experiment. We observe that the WALP helices assume tilted conformations and that lipid bilayers deform and change shape due to the interaction with the peptide. In accord with the hydrophobic matching hypothesis, we observe a monotonic variation of lipid boundary thickness as a function of peptide length. Helix tilt, however, as well as the average bilayer thickness show a more complex behavior.

Bilayer Structure Is Perturbed Differently by Different WALP Lengths. The lipid bilayer is not just a slab of hydrocarbon but consists of broad, overlapping distributions of various molecular components: headgroup, glycerol, and acyl chain segments which include methylene and terminal methyl groups.[52,62] We have therefore calculated a number of additional structural properties besides D_{PP}, to describe the molecular packing along the bilayer normal. In Figure 5, going from the headgroup regions toward the bilayer center, we have plotted the separations between lipid phosphorus atoms (D_{PP}), lipid glycerol C_2 carbons (D_{GG}), lipid monolayer centers of mass (D_{CM}), and acyl chain terminal methyls

(60) Brown, M. F.; Thurmond, R. L.; Dodd, S. W.; Otten, D.; Beyer, K. *Biophys. J.* **2000**, *78*, 409A.
(61) Lundbæk, J. A.; Andersen, O. S. *Biophys. J.* **1999**, *76*, 889−895.
(62) Huster, D.; Gawrisch, K. *J. Am. Chem. Soc.* **1999**, *121*, 1992−1993.

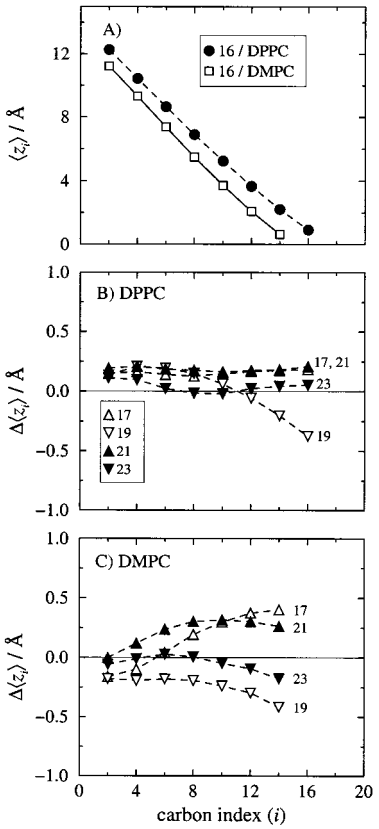

Figure 6. (A) Average acyl chain carbon positions, $\langle z_i \rangle$, as a function of carbon index i (averaged over both *sn*-1 and *sn*-2 chains) for WALP16/DMPC (open squares) and WALP16/DPPC (solid circles) relative to the bilayer center ($z = 0$). For easy comparison, the results from the other WALP*n* simulations in DMPC and DPPC are given relative to WALP16/DMPC (B) and WALP16/DPPC (C), respectively. Due to the peptide helical effect, there are similarities between WALP17 and WALP19 and WALP21 and WALP23 curves.

(D_{MM}). The most striking result in Figure 5 is the periodic variation of the structural parameters with the length of the peptide sequence. This zigzag shape propagates across the entire bilayer thickness from the bilayer center to the lipid headgroup. A closer inspection reveals that this periodic feature modulates a global, systematic increase with the peptide length, most clearly seen on the behavior of the center of mass separation D_{CM}. The periodicity effect is attenuated at the lipid−water interface as compared to the monolayer−monolayer interface at the bilayer center. This complex behavior is the result of a combined dependence on both peptide length and helical periodicity, as we show below. Also of note is that the difference between the two lipids, DMPC vs DPPC is minimal at the bilayer center and increases toward the headgroup region, a typical feature of saturated phosphatidylcholines.[63]

A more detailed description of the bilayer structure is provided by the acyl chain carbon average positions, $\langle z_i \rangle$, as a function of carbon index i. These $\langle z_i \rangle$ profiles carry information on both acyl chain tilt and segmental conformations. In particular, a deviation from a straight line (i.e. nonzero curvature) indicates a variation of segmental disorder along the acyl chain, as discussed in detail elsewhere.[63,64] Part A of Figure 6 compares the $\langle z_i \rangle$ curves for DMPC and DPPC in the presence of WALP16. The reference $z = 0$ value was set at the bilayer center in each case. In both cases, the acyl chain disorder increases toward the bilayer center, as indicated by the curved profiles. For easy comparison, the results for WALP17 to 23, shown in in parts B and C of Figure 6, are given relative to the WALP16 curves from part A. Specifically, the differences $\Delta\langle z_i \rangle \equiv \langle z_i \rangle - \langle z_i \rangle^{WALP16}$ are plotted. The nonmonotonic deviations along the acyl chains indicate differences in acyl chain conformations between the various WALP systems. For reference, a flat difference profile would indicate a global shift of the lipid molecules along the bilayer normal, while a straight line would in general indicate a change of acyl chain tilt. The results in parts B and C of Figure 6 show that the lipid acyl chains are more disordered in the case of WALP17 and WALP21 and less disordered in the case of WALP19 and WALP23 when compared to WALP16 systems. Note that the data points for the last acyl carbons (ω-carbons) on these curves correspond to the D_{MM} data points shown before in Figure 5. Figure 6 now gives the entire chain profile. The results reveal strong similarities between WALP17 and WALP21 systems, and (to a lesser extent) between WALP19 and WALP23, pointing to a periodic helical effect on the lipid bilayer structure.

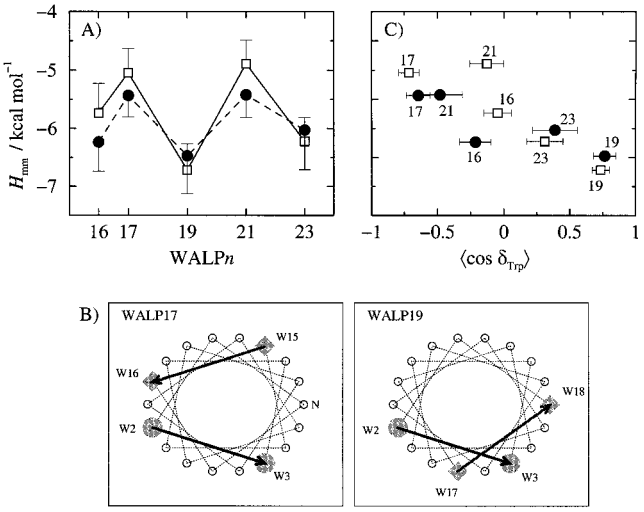

Figure 7. (A) Inter-monolayer interaction (H_{mm}) as a function of sequence length. Root-mean-square fluctuations are indicated with vertical bars. (B) Wheel diagrams based on ideal α-helices. The relative arrangement of Trp residues is indicated by the two solid line vectors in each panel (e.g. W3−W4 and W15−W16 for WALP17). The angle between these vectors (δ_{Trp}) changes with the number of intermediate residues. (C) Same data as in part A plotted versus the average $\langle \cos \delta_{Trp} \rangle$. Root mean-square fluctuations of $\cos \delta_{Trp}$ are indicated with horizontal bars. Stronger inter-monolayer interaction is seen for the WALP19 and WALP23 systems, as opposed to WALP17 and WALP21. Bilayers are more rigid for WALP19 and WALP23 for which all four Trp residues are roughly on the same side of the helix ($\cos \delta_{Trp} \geq 0$).

An energetic measure of the structural modulation in Figures 5 and 6 is provided by the interaction strength between the two opposed lipid monolayers. Part A of Figure 7 shows the trajectory averaged inter-monolayer interactions, denoted as H_{mm}. The peptide insertion perturbs the inter-monolayer coupling at the bilayer center in accord with the structural results presented in Figure 5. Stronger inter-monolayer interactions are seen for WALP19 and WALP23 than for WALP17 or WALP21. As we will discuss next, we attribute this helical effect mainly to the presence of Trp residues. On the basis of the extensive experimental evidence, the Trp residues are expected to strongly influence peptide interactions with lipid bilayers.[3,40,41,65]

(63) Petrache, H. I.; Dodd, S. W.; Brown, M. F. *Biophys. J.* **2000**, *79*, 3172−3192.

(64) Petrache, H. I.; Tu, K.; Nagle, J. F. *Biophys. J.* **1999**, *76*, 2479−2487.

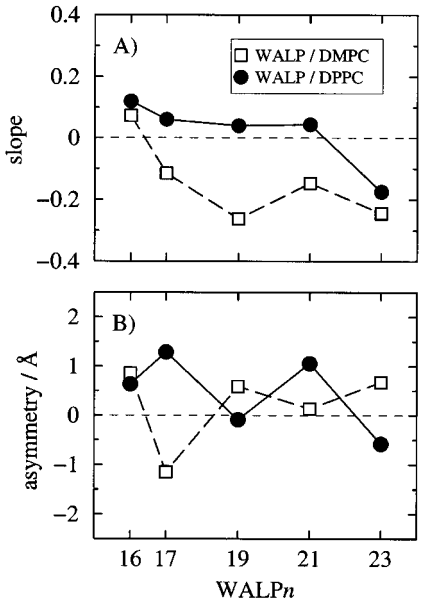

Figure 8. Lipid bilayer deformation next to the peptide (i.e. boundary conditions for the bilayer shape) as a function of WALP sequence length, n: (A) bilayer thickness slope $\Delta D_{PP}/\Delta r$; (B) bilayer asymmetry (difference between z_P^{upper} and $|z_P^{lower}|$), as explained in the text. The center of the bilayer ($z = 0$ plane) is defined by the location of the center of mass of the lipid molecules. DMPC results are shown with open squares, and DPPC results, with solid circles. Note the helical effect on bilayer deformation due to the peptide.

WALP sequences with different lengths would place the Trp residues at various locations along the bilayer normal. At the same time, by construction, different peptides will have different Trp arrangement around the helix axis. This variable Trp arrangement is indicated in part B of Figure 7 for two contrasting cases, WALP17 and WALP19. On the basis of the ideal α-helices (3.6 residues/turn), the two vectors defined by the Trp pairs at the N-terminus and the C-terminus, respectively are, roughly, antiparallel in the case of WALP17 and parallel for WALP19. From a structural point of view, WALP17 has the Trp pairs on opposite sides of the helix axis, while WALP19 has them on the same side. To show correlations between Trp arrangements and the structure of the surrounding lipid bilayer, we have defined a Trp "arrangement angle", denoted by δ_{Trp}, as the angle between the two Trp vectors in Figure 7B. In part C of Figure 7 we then replot the inter-monolayer interactions H_{mm} from part A, this time as a function of $\langle \cos \delta_{Trp} \rangle$. The average is calculated over the actual δ_{Trp} values in each of the simulations. This correlation plot places the data points at negative $\langle \cos \delta_{Trp} \rangle$ for WALP17 and WALP21, positive $\langle \cos \delta_{Trp} \rangle$ for WALP19 and WALP23, and roughly zero for WALP16. Note that DMPC and DPPC data show similar $\langle \cos \delta_{Trp} \rangle$ values, except for WALP21 and WALP16, for which some possible backbone distortion has occurred. The inter-monolayer interaction is strongly correlated with the Trp angle, δ_{Trp}, and shows that stronger coupling exists in the case of WALP19 and WALP23 (tryptophans on the same side) than for WALP17 or WALP21 (tryptophans on opposite sides).

A helical effect is also seen on the bilayer shape. Figure 8 shows the slope and the asymmetry of the perturbation profile induced by the peptide insertion. The slope shown in part A is calculated as the variation of D_{PP} with the in-plane distance r from the peptide and is, therefore, a dimensionless quantity. A positive/negative slope indicates a thinning/thickening of the bilayer next to the peptide. The asymmetry parameter in part B is calculated as the difference between monolayer thicknesses at the peptide−lipid interface. More precisely, if we denote the average position of phosphorus atoms of boundary lipids in the two monolayers (upper and lower) by z_P^{upper} and z_P^{lower}, then the boundary bilayer thickness is given by $D_{PP}^b = z_P^{upper} + |z_P^{lower}|$, and the asymmetry is $z_P^{upper} - |z_P^{lower}|$. From Figure 8, we note the periodic helical effect on both the slope and asymmetry results. Part A shows that the slope changes sign from positive to negative as the peptide becomes longer; i.e., above some peptide length threshold, the bilayer starts getting thicker instead of thinner next to the peptide. This length threshold is between WALP16 and WALP17 for DMPC and between WALP21 and WALP23 for DPPC, in accordance with the results for D_{PP} and D_{PP}^b shown before in Figure 4. In addition, the asymmetry parameter shown in part B of Figure 8 shows that the symmetry about the bilayer midplane present in a pure lipid bilayer is disrupted by the peptide. This can be due to the peptide backbone helicity or be enhanced by the inherent asymmetric arrangement of the Trp residues relative to helix axis (see below). It is clear that peptide−lipid bilayer interactions make the two monolayers inequivalent.

In-Plane Packing: Area/Peptide Increases with Peptide Length. Having discussed the structural properties along the bilayer normal, we now turn to in-plane molecular packing. Lipid bilayers are fluid systems, and consequently, longitudinal deformations are counterbalanced by lateral molecular arrangements. Due to the total area of the membrane system being fixed during the simulation, the relevant quantity to consider is the area *redistribution* between the peptide and the lipids in each simulation box. There is however a technical complication in defining molecular areas within heterogeneous systems, as for the calculation of molecular components volumes.[66] As mentioned earlier (see Methods), the peptide area is not an intrinsic property but depends on the interaction with the environment. Therefore, it should be calculated as the change in the total membrane area upon addition of extra peptide. This procedure, however, would require a major computational effort. As a more suitable alternative for our present simulations, we have followed an approach used for the analysis of bilayer electron density profiles obtained from X-ray scattering (Luzzati method; see review by Nagle and Tristram-Nagle[54]). In this approach, we first calculate the volumetric membrane thickness,

$$D_B = \frac{V_{box} - V_{water}}{A_{box}}, \qquad (1)$$

where the difference $V_{box} - V_{water}$ represents the membrane volume (peptide plus lipids, no water). Then using D_B and the molecular volumes for the peptide (V_P) and lipid (one molecule, V_L), we define the average molecular areas as

$$\langle A_P \rangle = \frac{V_P}{D_B} \qquad (2)$$

and

(65) Andersen, O. S.; Greathouse, D. V.; Providence, L. L.; Becker, M. D.; Koeppe, R. E. *J. Am. Chem. Soc.* **1998**, *120*, 5142−5146.

(66) Petrache, H. I.; Feller, S. E.; Nagle, J. F. *Biophys. J.* **1997**, *72*, 2237−2242.

$$\langle A_L \rangle = \frac{2V_L}{D_B} \quad (3)$$

where $\langle A_P \rangle$ and $\langle A_L \rangle$ are the average lateral areas of the peptide and lipid molecule, respectively. This procedure has the advantage that the molecular areas so calculated can be consistently compared across different simulations. Also note that this procedure preserves the conservation relationship $\langle A_P \rangle + N_L \langle A_L \rangle = A_{box}$, where N_L represents the number of lipids in one monolayer.

We first present the volumetric results needed for the area calculations. We have calculated peptide volumes (V_P) using a 3D Voronoi algorithm developed by Gerstein et al.,[67] previously used for other similar peptide−lipid systems.[30] The lipid volumes (V_L) are calculated by subtracting V_P and the water volume (V_{water}) from the total cell volume (V_{box}) and dividing by the number of lipids in the unit cell. The water density for the simulated systems is 0.0334 Å^{-3} (30 °C) and 0.0329 Å^{-3} (50 °C) and was extracted from the water region plateau.[66] The results are given in Table 3. First, we note that lipid volumes agree very well (0.5% deviation) with the experimental measurements of 1101 Å^3 for DMPC at 30 °C[50] and 1232 Å^3 for DPPC at 50 °C.[51] Second, the peptide volume increases monotonically with the sequence length, as expected, due to the additional Ala and Leu residues. Compared to the lipid molecules, the peptide volumes are 2−3 times as large. Further comparison in terms of the material properties can be made on the basis of mass densities calculated as a ratio between molecular mass and volume. We find that the peptide material, with a mass density of 1.14 g/mL, is much denser than water (0.99 g/mL at 30 °C) as well as lipid (1.03 g/mL for DMPC at 30 °C). The WALP molecules are 14% heavier than water, compared to 3% for DMPC.

If we return to the area results, the computed molecular cross-sectional areas $\langle A_P \rangle$ and $\langle A_L \rangle$ are given in Table 3 and show that $\langle A_P \rangle$ increases with peptide length at the expense of the area/lipid $\langle A_L \rangle$. The lipids surrounding longer peptides are more stretched longitudinally (as seen in Figure 4) making the area/lipid $\langle A_L \rangle$ smaller. Clearly, due to the total area being fixed, the area redistribution among peptide and lipids is such that the sum $A_P + N_L A_L$ is conserved (see Methods). That $\langle A_P \rangle$ increases with increasing WALP length can be immediately seen from its defining relationship in eq 2. While the peptide volume V_P increases steadily with increasing number of residues, the volumetric membrane thickness D_B increases less dramatically, as seen in Table 3. At present, there is no experimental measurement on either $\langle A_P \rangle$ or $\langle A_L \rangle$ for mixed WALP−lipid systems. There is however data on the lipid area in pure lipid bilayers, which we have used to construct the simulation box (cf. Methods). The values used were $A^0_{DMPC} = 59.7$ Å^2 [50] and $A^0_{DPPC} = 62.9$ Å^2,[51] where the superscript indicates pure (unperturbed) lipid bilayers. In addition, we used a value for the peptide area (see Methods), which now, in retrospect, appears to be an overestimate. During the simulation, an area redistribution between the peptide and the lipids occurred such that $\langle A_P \rangle$ decreased and the area/lipid $\langle A_L \rangle$ increased. In reference to pure lipid bilayers, the areas/lipid $\langle A_L \rangle$ that we obtain for the WALP−lipid systems are larger by 14.0−10.8% for DMPC (WALP16−23) and by 14.3−11.4% for DPPC. While these might be an overestimate for WALP−lipid systems, we note that lipid areas on the order of 70 Å^2 for DMPC and DPPC (as in Table 3) have been experimentally measured in some circumstances, such as increased temperature.[63] Thus, the observed increment on the area/lipid is safely within the expansion limits of phosphatidylcholine membranes. We also find that DPPC molecules are laterally stretched more than DMPC, making the effective area/peptide smaller in the DPPC systems. This implies that, for similar lateral packing, the starting area for WALP should have been about 5% smaller in DMPC (or, alternatively, 5% larger in DPPC), to account for differences in the temperature and lipid lateral density. This problem can in principle be avoided by using constant lateral pressure (surface tension) boundary conditions and letting the lateral area relax to an equilibrium value (see Methods). This approach, however, can be computationally demanding, especially if the starting area is far from equilibrium or if the applied lateral pressure is not appropriate for the simulated system size, as discussed by Feller and Pastor.[44] It is therefore advantageous to start with a set of constant area simulations for faster equilibration to gain initial insights into peptide−lipid packing. Surface tension values, calculated as overall trajectory averages, are given in the last column of Table 3. We also note that, due to the small system size, fluctuations in the surface tension are relatively large. Block averaging on 50 ps time windows gives root mean-square deviations on the order of 10−20 dyn/cm, while instantaneous values deviate by roughly 200 dyn/cm in average. The values given in Table 3 are typical for simulations of small bilayer patches which, by construction, are constrained to remain flat.[44]

Table 3. Volumetric Results and Surface Tension Values

lipid	WALP	V_P[a]	V_L[b]	D_B[c]	$\langle A_P \rangle$[d]	$\langle A_L \rangle$[e]	γ[f]
DMPC	16	2732	1095	31.99	85.4	68.4	25
(30 °C)	17	2906	1089	32.00	90.8	68.1	21
	19	3212	1087	32.21	99.7	67.5	32
	21	3475	1104	32.92	105.6	67.1	48
	23	3756	1097	32.98	113.9	66.5	26
DPPC	16	2751	1221	33.95	81.0	71.9	22
(50 °C)	17	2948	1221	34.12	86.4	71.6	32
	19	3229	1222	34.39	93.9	71.1	30
	21	3501	1228	34.78	100.7	70.6	38
	23	3788	1229	35.05	108.1	70.1	48

[a] Average peptide volume. [b] Average lipid volume. [c] Volumetric membrane thickness (eq 1). [d] Average cross-sectional area/peptide (eq 2). [e] Average cross-sectional area/lipid (eq 3). Length units are Å. [f] Surface tension values (in units of dyn/cm) calculated from the trajectories.

Discussion

General Aspects of Hydrophobic Matching. There is increasing evidence that membrane protein conformations are modulated by the interaction with the lipid environment.[15] In particular, the orientation and flexibility of the transmembrane domain conferred by the surrounding lipid bilayer are expected to play a role in protein function. The protein insertion, in turn, affects the lipid bilayer and modifies its physical properties. How can one investigate such a complex mechanism to understand its implications for protein function? Molecular dynamics simulations are well suited for modeling interactions in multicomponent systems to help with the interpretation of experimental measurements such as X-ray, NMR, and infrared spectroscopy. A more practical description of the hydrophobic matching mechanism, however, requires a reduction from a many-body problem to a tractable (phenomenological) representation involving a reduced number of degrees of freedom. Current models treat the

(67) Gerstein, M.; Tsai, J.; Levitt, M. *J. Mol. Biol.* **1995**, *249*, 955−966.

lipid bilayer as elastic plates that can sustain bending and compression deformations. The peptide molecule (typically a helical structure) is in turn modeled as a linear spring described by a characteristic spring constant and equilibrium (undeformed) length and cross section.

In the present simulations we have systematically varied the equilibrium (unperturbed) dimensions of both peptide and lipid bilayer and monitored the effects on helix tilt and bilayer deformations. In doing so, we have identified an additional relevant degree of freedom, in the case of WALP systems, namely the relative arrangement of Trp residues along the helical axis. Due to the helical structure of the peptide, Trp placement (quantified by the angle δ_{Trp}) varies as the number of intervening residues is modified. This leads to an observable helical (periodic) effect on the structure and dynamics of the peptide−lipid bilayer system. Experimental results[35] have indicated that, indeed, peptide tilt has a complex behavior as a function of peptide length, and a comparison between experiment and simulation was provided in Figure 3. Although we are cautious in interpreting the quantitative results, both simulation and experiment agree on the qualitative aspect of the data indicative of a helical effect. It is also worth noting that experimental studies of these peptides in model membranes of phosphatidylethanolamine suggest that a similar helical effect might occur on the lamellar-to-isotropic phase transition at intermediate peptide concentration.[68]

Interpretation of Simulation Results. In general, simulation results, as well as experimental results for that matter, require theoretical interpretation. In particular, simulated membrane systems are inherently limited in both time and length scale, while real membranes exhibit a wide dynamic range. The characteristic time domain of the lipid membrane motions extend from isomerization transitions (picoseconds) to lipid diffusion (microseconds), to lipid flip-flop across the bilayer (possibly seconds).[69] Sizewise, lipid molecules show uncorrelated local motions (e.g. protrusion into the water space) leading to the characteristic bilayer roughness, as well as collective (correlated) motions that lead to bilayer undulations at lengthscales up to fraction of a micrometer.[70−74] Why should we then consider nanosecond molecular dynamics simulations of small bilayer patches? As demonstrated by Berendsen and co-workers at the onset of molecular dynamics studies,[31,75,76] many features of the lipid bilayers have been elucidated even from minimal membrane sizes (nanometers) and short time scales (tens of picoseconds). One typical example is the understanding of the origin of the acyl chain order profile measured by ^{2}H NMR spectroscopy in terms of chain conformations and packing. It has been generally shown that valid qualitative, if not quantitative, results can emerge from careful investigation of simulation results. Clearly, many of the dynamic features of the real membrane are currently not within computational reach. The simulation field, however, is continuously evolving and making progress toward longer time and length scales.[74,77−79]

As a rule, the problem addressed and the computing power available determine the length of the simulation. Therefore, for a project involving multiple simulations, as for the WALP series in this work, one needs to find the optimum compromise between the number of trajectories and their length. In this study we have considered structural deformations imposed on the lipid bilayer upon insertion of hydrophobic peptides. The relevant molecular motions involved, namely peptide tilt and lipid rearrangement, are minimally sampled within nanosecond time scales, meaning that random (sampling) errors are large. However, a detailed comparison across multiple WALP systems enables us to extract meaningful conclusions more so than from individual longer trajectories. This is because systematic errors (e.g. due to choice of boundary conditions and finite size effects) have a reduced influence on the trends observed. In addition, we have found that longer trajectories (10 ns for WALP19/DMPC and 5 ns for WALP23/DMPC) give average structural parameters as well as fluctuation ranges that do not differ significantly from the initial 1.25 ns windows. We should emphasize that careful preparation of the initial state as well as constrained-equilibration stages (cf. Methods) is a prerequisite for fast overall equilibration and adequate sampling during production dynamics. Although simulations of lipid bilayers have often been successful in reproducing experimental results, the comparison with experiment is not always straightforward. Our present simulations, for instance, are carried out at constant lateral area, while the experimental measurements most likely correspond to a constant lateral pressure situation. This means that, in reality, peptide tilt relaxation can be coupled with large scale area fluctuations and lateral stretching, as opposed to just local fluctuations occurring under constant total area restraint. In addition, bilayer undulations are absent in the simulation but could influence the experimental result.[44,74] With the possibility of bilayer undulations being coupled with lateral fluctuations, one might expect an influence on peptide tilt and cross-sectional area of both peptide and lipid molecules. Obviously, further analysis on longer trajectories and larger systems is required for better comparison with experiment. In this regard, one notes that while the simulated peptide:lipid concentration is the same as for the experiments,[18,35,41] the simulated systems do not account for possible effects of peptide−peptide interactions, which could lead to peptide aggregation and domain formation and more complex dynamics in general. Unfortunately, the addition of more peptide molecules at constant peptide:lipid concentration quickly generates prohibitive system sizes. Simulation results, therefore, almost always require theoretical interpretation. Let us note that most experimental measurements also require theoretical interpretation, as is presently the case for the conversion of FTIR data into peptide tilt values shown in Figure 3. The assumptions involved introduce inherent approximations as discussed by Bechinger et al.[59] and de Planque et al.[35] These assumptions, however, could be tested by simulations, further emphasizing the interplay between experiment and simulations.

Role of Trp on Peptide−Lipid Bilayer Structural Matching. Structural parameters, as well as interaction

(68) Morein, S.; Koeppe, R. E.; Lindbom, G.; de Kruijff, B.; Killian, J. A. *Biophys. J.* **2000**, *78*, 2475−2485.
(69) Pastor, R. W.; Feller, S. E. In *Biological Membranes*; Merz, K., Roux, B., Eds.; Birkhäuser: Boston, MA, 1996; pp 3−29.
(70) Helfrich, W. *Z. Naturforsch.* **1978**, *33a*, 305−315.
(71) Evans, E.; Rawicz, W. *Phys. Rev. Lett.* **1990**, *64*, 2094−2097.
(72) Hołyst, R. *Phys. Rev. A* **1991**, *44*, 3692−3709.
(73) Nevzorov, A. A.; Brown, M. F. *J. Chem. Phys.* **1997**, *107*, 10288−10310.
(74) Lindahl, E.; Edholm, O. *Biophys. J.* **2000**, *79*, 426−433.
(75) van der Ploeg, P.; Berendsen, H. J. C. *J. Chem. Phys.* **1982**, *76*, 3271−3276.
(76) van der Ploeg, P.; Berendsen, H. J. C. *Mol. Phys.* **1983**, *49*, 233−248.
(77) Feller, S. E.; Huster, D.; Gawrisch, K. *J. Am. Chem. Soc.* **1999**, *121*, 8963−8964.
(78) Chiu, S.-W.; Clark, M.; Subramaniam, S.; Jakobsson, E. *J. Comput. Chem.* **2000**, *21*, 121−131.
(79) Tieleman, D. P.; Berendsen, H. J. C.; Sansom, M. S. P. *Biophys. J.* **2001**, *80*, 331−346.

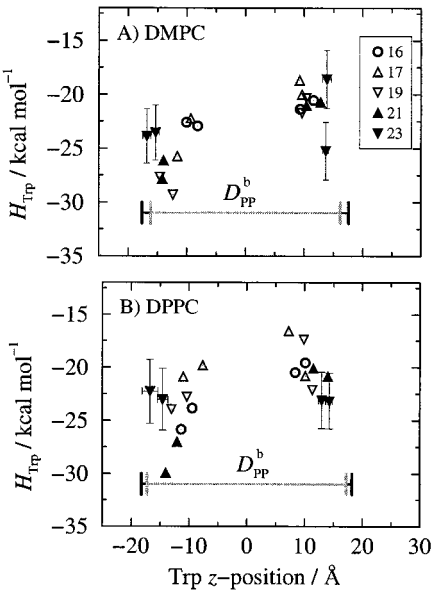

Figure 9. Trp interaction (includes the C_α carbon) with the environment (H_{Trp}) vs average center of mass location along the bilayer normal in DMPC (A) and DPPC (B). Trp−environment interactions are stronger at the lipid−water interface. Systematically stronger interactions are seen for Trp residues at the N-terminus (negative z). The vertical and horizontal bars indicate mean-square fluctuations during 1.25 ns of simulated trajectories (shown only for WALP23 for clarity). The bottom horizontal lines show the range of boundary bilayer thickness (D^b_{PP}) from WALP16 to WALP23.

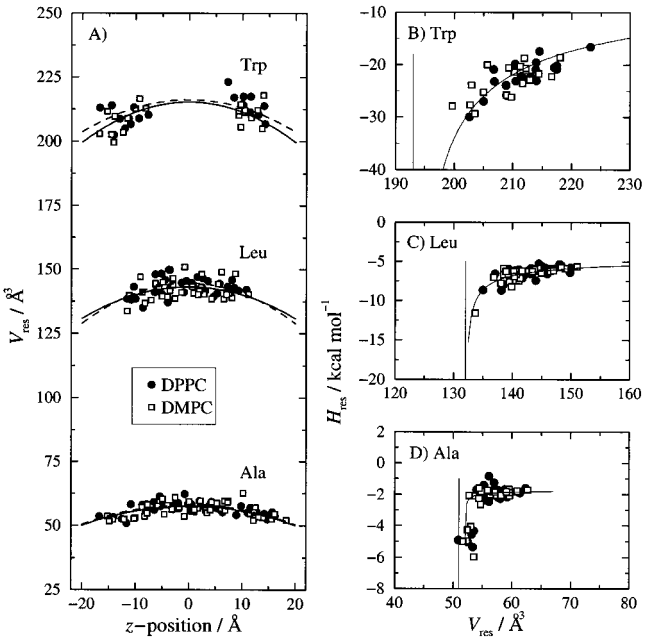

Figure 10. (A) Peptide side chain volumes (V_{res}) as a function of average location along the bilayer normal ($z = 0$ set at the bilayer center). Chemically equivalent side chains have larger volumes at the bilayer center, corresponding to the bilayer density gradient along the bilayer normal. The solid and dashed lines are harmonic fits to the data points for DMPC and DPPC, respectively. (B−D) Trajectory-averaged side chain−environment interactions (H_{res}) vs V_{res} for Trp (B), Leu (C), and Ala (D) side chains. The data are fit with empirical H_{res} vs V_{res} curves, and the vertical lines indicate bare volumes (steric limits) as explained in the text.

terms such as the inter-monolayer interaction, suggest that WALP helices with the Trp pairs on the same side (WALP19 and 23) behave differently than peptides with Trp pairs on opposite sides (WALP17 and 21). In particular, the latter have a tendency for larger peptide tilt angles. The tilt angles, however (and other structural parameters), have a complex behavior determined by both peptide length and δ_{Trp}. This shows the complexity of structural deformations occurring within the WALP−lipid system. Since different peptides might place the Trp residues at different locations along the bilayer normal, we have looked at the interaction between Trp side chains and the environment (lipid and water). These are shown in Figure 9. There is clearly a strong dependence of Trp interaction with the environment (lipid + water) as a function of average position along the bilayer normal. Similar results have been obtained for Trp analogues, indole and *N*-methylindole, inserted in POPC bilayers.[53] Figure 9 also shows a clear asymmetry between the two monolayers. When one is looking at these results, it helps to recall the molecular heterogeneity along the bilayer normal. This heterogeneity gives rise to both a hydrophobic gradient as well as a mass density gradient. The two physicochemical properties are obviously interconnected, but it is useful to make a distinction between chemical and molecular packing heterogeneity. The Trp residues have bulky side chains, and therefore, the packing density in their vicinity is relevant to our understanding of the peptide−lipid bilayer matching. For this reason, a convenient quantity to consider is the side chain volume,[30] as we discuss next.

Part A of Figure 10 shows trajectory averaged side chain volumes as a function of average position along the bilayer normal. The volumes are calculated using a Voronoi procedure[67] and include all residue atoms except the peptide bond. Figure 10A highlights the magnitude of Trp volumes compared with the smaller Leu and Ala side chains. The Trp volumes, on the order of 210 Å^3, are almost comparable with the lipid headgroups, which are of about 320 Å^3.[66,80] For this reason, the Trp residues have a significant effect on the molecular crowding at the lipid−water interface. The figure shows all volumetric data superimposed, although the DMPC and DPPC simulations are performed at different temperatures. The main aspect to notice is that the side chain volumes show a positional dependence corresponding to the bilayer density gradient: chemically equivalent side chains have larger volumes at the bilayer center. The superposition of all data allows an easy comparison between the z- and T-dependence. Incidentally, the data in this range can be fit with simple harmonic functions, as shown by the solid (DMPC) and dashed (DPPC) curves in part A of Figure 10. As the headgroup region is approached ($|z| > 10$ Å), there are noticeable deviations from the fitted lines, especially for the Trp residues, reflecting the interactions with the lipid headgroups. Upon close inspection, the behavior of Trp volumes as a function of z-position resembles the interaction with the environment shown previously in Figure 9. This is better seen by directly plotting the side chain interaction with the environment (enthalpy, H_{res}) vs side chain volume, V_{res}, as shown in part B of Figure 10. For comparison, the results for Leu and Ala residues are also presented in parts C and D, respectively. The location and curvature of the H_{res} vs V_{res} curves changes, with a shift toward smaller V_{res} and $|H_{res}|$ from Trp to Leu to Ala side chains. Bare volumes (steric limits, V_0) are indicated by the vertical lines in each panel, and the data points are fit using an empirical function $H - H_0 = a(V - V_0)^b$ with $b = -1/2$. A more detailed analysis

(80) Armen, R. S.; Uitto, O. D.; Feller, S. E. *Biophys. J.* **1998**, *75*, 734−744.

of these H_{res} vs V_{res} curves, in relation with the lipid bilayer density gradient, might help further refinement of hydrophobic matching models.

Conclusions

Molecular dynamics simulations of the WALP*n* series (with $n = 16$, 17, 19, 21, and 23) incorporated in two lipid bilayer types (14 and 16 acyl chain carbons, respectively) has revealed intriguing aspects of the hydrophobic matching mechanism and the critical role of the tryptophan side chains. As expected, the Trp side chains have a significant effect on the dynamic structure of both peptide and lipid bilayer. On the basis of a detailed volumetric analysis, we have demonstrated the role played by the density gradient along the bilayer normal on the peptide−lipid structural matching. Due to their large size, the Trp side chains at the ends of the peptide perturb the molecular packing at the lipid−water interfaces. Interestingly, their effect is not only local but is transmitted across the bilayer and affects the inter-monolayer coupling at the bilayer center. We have found that the peptide−lipid packing, and in particular the peptide tilt, depend not only on peptide length but also on the relative positions of Trp residues around the helix axis, measured by the Trp arrangement angle, δ_{Trp}. This represents an additional structural property that modulates the hydrophobic matching in the case of WALP systems, showing that details of the peptide structure influence peptide tilt and bilayer deformations. We find that WALP structures with all four Trp residues on the same side of the helix couple more strongly with the surrounding lipid bilayer than do peptides with Trp residues on opposite sides. These observations may guide further analysis on membrane proteins and their interaction with the lipid environment.

Abbreviations

DMPC	dimyristoylphosphatidylcholine
DPPC	dipalmitoylphosphatidylcholine
WALP	tryptophan-alanine-leucine peptide

Acknowledgment. We thank Richard W. Pastor for valuable discussions and for critical reading of the manuscript. We also thank Alan Grossfield for assistance with analysis scripts and most useful suggestions. This work was supported by funds from the NIH, Bard Foundation, and the Department of Physiology at The Johns Hopkins University School of Medicine.

LA011338P